Research paper

The Holocene
2016, Vol. 26(4) 567–577

DOI: 10.1177/0959683615612566
hol.sagepub.com
SAGE

# Holocene land–sea climatic links on the equatorial Pacific coast (Bay of Guayaquil, Ecuador)

**Brice Seillès,[1] Maria Fernanda Sánchez Goñi,[1] Marie-Pierre Ledru,[2] Dunia H Urrego,[1,3] Philippe Martinez,[4] Vincent Hanquiez[4] and Ralph Schneider[5]**

**Abstract**

We analyzed the pollen content of a marine core located near the Bay of Guayaquil in Ecuador to document the link between sea surface temperatures (SSTs) and changes in rainfall regimes on the adjacent continent during the Holocene. Based on the expansion/regression of five vegetation types, we observe three successive climatic patterns. In the first phase, between 11,700 and 7700 cal. yr BP, the presence of a cloud (Andean) forest in the mid altitudes and mangroves in the estuary of the Guayas basin, were associated with a maximum in boreal summer insolation, a northernmost position of the Intertropical Convergence Zone (ITCZ), a land–sea thermal contrast, cloud dripping, and dry edaphic conditions. Between 7700 and 2850 cal. yr BP, the expansion of the coastal vegetation and the regression of the mangrove indicate a drier climate with weak ITCZ and low El Niño Southern Oscillation (ENSO) variability while austral summer insolation gradually increased. The interval between 4200 and 2850 cal. yr BP was marked by the coolest and driest climatic conditions of the Holocene because of the weak influence of the ITCZ and a strengthening of the Humboldt Current. After 2850 cal. yr BP, high variability and amplitude of the Andean forest changes occurred when ENSO frequency and amplitude increased, indicating high variability in land–sea connections. The ITCZ reached the latitude of Guayaquil only after 2500 cal. yr BP inducing the bimodal precipitation regime we observe today. Our study shows that besides insolation, the ITCZ position, and ENSO frequency, changes in eastern equatorial Pacific SSTs play a major role in determining the composition of the ecosystems and the hydrological cycle of the Ecuadorian Pacific coast and the Western Cordillera in Ecuador.

**Keywords**

Ecuador, El Niño Southern Oscillation, Holocene, Humboldt Current, Intertropical Convergence Zone, Pacific sea surface temperature, Western Cordillera

Received 21 May 2015; revised manuscript accepted 14 September 2015

## Introduction

The equatorial Eastern Pacific coast represents one of the largest desert areas of the planet. This desert stops abruptly on the Peruvian–Equatorial margin, between 1°S and 3°S latitude, where within a few kilometers of distance, it is suddenly replaced by a luxuriant and diverse tropical rainforest (Barthlott et al., 2005). This contrasted biogeographical pattern is created by the boundary effect of the position of the Intertropical Convergence Zone (ITCZ) from the north, and by the intensity of the cold Humboldt Current from the south (Jorgensen and Leon-Yanez, 1999). The interplay between the northern and the pole–equator Southern Hemisphere (SH) seasonal insolation and pole–equator temperature gradient controls the position and amplitude of the ITCZ, oscillating between 10°N and 3°S, and the characteristic bimodal regional rainfall distribution of the tropics (Garreaud et al., 2009). Today, the cooling of surface waters in the southeastern equatorial Pacific during the austral winter, displaces the sea surface temperature (SST) maximum (and thus the zone of convergence) into the Northern Hemisphere (NH), and inversely during the austral summer. Superimposed to this ocean–atmospheric coupling, the climate is regularly submitted to the interannual variability of the El Niño Southern Oscillation (ENSO) (Garreaud et al., 2009; Schneider et al., 2014; Vuille et al., 2000). On the equatorial Eastern Pacific, ENSO is characterized by an abrupt change in SST that affects the amplitude of the seasonal shifts of the ITCZ or the location of the northernmost limit of influence of the Humboldt Current that will control the hydrological cycle on the continent (Garreaud et al., 2009; Leduc et al., 2009).

Seasonal shifts of the ITCZ during the Holocene are well documented on the northern coast of Venezuela (Haug et al., 2001). The seasonally varved marine record of Cariaco off the coast of

[1]Ecole Pratique des Hautes Etudes (EPHE), UMR-CNRS 5805 EPOC, University of Bordeaux, France
[2]IRD, UMR 226, Institut des Sciences de l'Evolution de Montpellier (ISEM) (UM CNRS IRD EPHE), France
[3]College of Life and Environmental Sciences, University of Exeter, UK
[4]UMR CNRS 5805 EPOC, University of Bordeaux, France
[5]Institute of Geosciences, University of Kiel, Germany

**Corresponding author:**
Maria Fernanda Sánchez Goñi, Ecole Pratique des Hautes Etudes (EPHE), UMR-CNRS 5805 EPOC, University of Bordeaux, Allée Geoffroy Saint-Hilaire, 33615 Pessac, France.
Email: mf.sanchezgoni@epoc.u-bordeaux1.fr

Venezuela indicates that the Holocene's wettest period between 10,500 and 5400 cal. yr BP, a period termed the Holocene Thermal Maximum, is related to a more northerly position of the ITCZ. This moist period is followed by large century-scale variations in precipitation between 3800 and 2800 cal. yr BP explained by increased frequency of ENSO events. Marine and terrestrial records off the Peruvian and Ecuadorian margin reveal that the ITCZ position also varied through time (Cane et al., 2005), and the hydroclimate was in anti-phase with that of the Cariaco basin (Mollier-Vogel et al., 2013). Superimposed to this long-term hydroclimate variability, millennial-scale ENSO events in the southern and northern tropics punctuated the Holocene. The frequency of these events increased from 7000 to 1000 cal. yr BP, with a 2- to 7-year cyclicity since 5000 cal. yr BP (Moy et al., 2002). The maximum of ENSO frequency was reached between 3500 and 2600 cal. yr BP (Haug et al., 2001; Riedinger et al., 2002), possibly in response to a threshold reached by the gradual decrease in boreal summer insolation (Clément et al., 2000; Rodbell et al., 1999), and leading to the observed marked aridity/humid trend at Cariaco/Guayas. Recent climate simulations showed that insolation is the major driver of SST changes in the equatorial Eastern Pacific and has a greater effect on seasonality and interannual variability since the beginning of the Holocene (Braconnot et al., 2012).

However, the processes and degree of coupling between, on the one hand, equatorial Eastern Pacific SST, rainfall distribution, and intensity on land and, on the other hand, insolation forcing, ITCZ position, and ENSO variability, are far from being understood. Here, we address this issue by presenting the first continuous marine pollen record of the equatorial Eastern Pacific margin and use the related changes in vegetation and SST to characterize the boundaries of the ITCZ and the Humboldt Current during the Holocene. This direct comparison between terrestrial and oceanic climatic tracers is an original approach for this complex region.

## Present-day environmental setting

### *Climate and oceanic circulation*

The climate of the Guayaquil region is controlled by seasonal shifts of the ITCZ. The rainfall distribution is bimodal with a 4-month rainy season (JFMA) when the ITCZ is located at the latitude of Guayaquil and a long dry season (JJASON) when the ITCZ is located further north (climate diagram in Figure 1). Consequently, today the maxima in precipitation and river discharge in the Guayaquil basin and Western Cordillera mid-elevation is observed during the austral summer (Rincón-Martínez et al., 2010). Further south, the rainfall distribution of the Pacific coast and of the western Andean Cordillera, from southern Perú until the latitude of Guayaquil, is under the influence of the Humboldt Current, a cold current that provokes upwelling along the western margin of the South American continent, maintaining a long line of coastal desert (Vuille et al., 2000). Aridity is found along the path of the cold Humboldt Current, which stabilizes the atmosphere under high pressures. The desert stops south of Guayaquil where the Humboldt Current is deviated to the west.

Anomalies in the seasonal pattern of rainfall distribution are observed during the ENSO, when the temperature gradient between the Eastern and Western Pacific is modified. This interannual variability shows two phases (Wyrtki, 1975): La Niña (cold) phase is characterized by SST decrease in the equatorial Eastern Pacific margin and drier climate on the continent; during the El Niño (warm) phase of the oscillation, the sea current is reversed leading to wind decrease in the equatorial Eastern Pacific and warm water along the Peruvian margin and more precipitation on the continent. ENSO is therefore the main cause of present-day climatic variability of these regions at the edge of the tropical Pacific Ocean (Moy et al., 2002; Tudhope et al., 2001). Additionally, previous results show that ENSO variability is more important for long-term climate characterization than considering separately the number of El Niño and La Niña events per year (interannual variability;Ledru et al., 2013; Morales et al., 2012).

### *Present-day vegetation and its pollen representation*

The Bay of Guayaquil is situated in a transitional zone generated by the interplay between the cold Humboldt Current and the equatorial warm current . As a result, the distribution of the ecosystems is divided into two main types: a desert vegetation cover in the south and a wet tropical forest with mangrove swamps in the north of the study area. Within the basin of Guayaquil, the distribution of the vegetation is subdivided into five main ecosystems (pie chart in Figure 1, Table 1). Their respective pollen indicator taxa have been grouped according to published pollen–vegetation calibration datasets (Ledru et al., 2013; Urrego et al., 2011) and list of plants (Jorgensen and Leon-Yanez, 1999):

1. The Andean forest refers to the evergreen and ombrophilous forests up to a mean elevation of 3600 m. This vegetation is essentially represented by *Podocarpus, Alnus, Morella* (*Myrica*), and *Myrsine*, and associated with cool and relatively wet environmental conditions all year round. *Alnus* occurs on wet soils along rivers in this montane forest but can also occur as swamp forest (carr) around water bodies (Marchant et al., 2002). Modern studies on the pollen representation of the Eastern Cordillera vegetation (Urrego et al., 2011) show that *Hedyosmum* is also a frequent component of this forest between 1500 and 3000 m a.s.l., although it also occurs in the Pacific forest.
2. The Pacific rainforest is composed of evergreen and semideciduous species and distributed between the coastal piedmont in the periphery of the mangrove swamp and the Western Cordillera. This forest is essentially represented by Urticaceae/Moraceae-type, and directly affected by the development (expansions and contractions) of the mangrove forest.
3. The coastal vegetation group is composed of desert shrubs and herbs and essentially represented by Chenopodiaceae/Amaranthaceae, *Acalypha*, and *Ambrosia peruana* that develop under cold and dry conditions.
4. The Páramos or high-elevation tropical grasslands are located above the upper forest line and are represented by *Acaena-Polylepis*-type and *Baccharis*-type that group all the Asteraceae tubuliflorae excluding *Ambrosia*-type.
5. The mangrove forest, essentially represented by *Rhizophora*, corresponds to coastal vegetation related to a wet and saline environment in the tropical and subtropical regions dominated by the equatorial warm current. It is impacted by the marine dynamics (sea level, tidal system, salinity) but also by hydric and nutrient contributions of the riverine runoff.

Pollen grains from these main vegetation types are mostly transported by the Guayas River as previous works (e.g. Heusser and Balsam, 1977) clearly show that cores located close to river mouth recruit preferentially pollen via fluvial transport. This is particularly true for this region where the dominant winds come from the ocean. Once in the sea, planktonic filter feeder organisms consume sinking debris (including pollen grains) and produce fecal pellets which have a greater sinking velocity in the water column (Hooghiemstra et al., 2006).

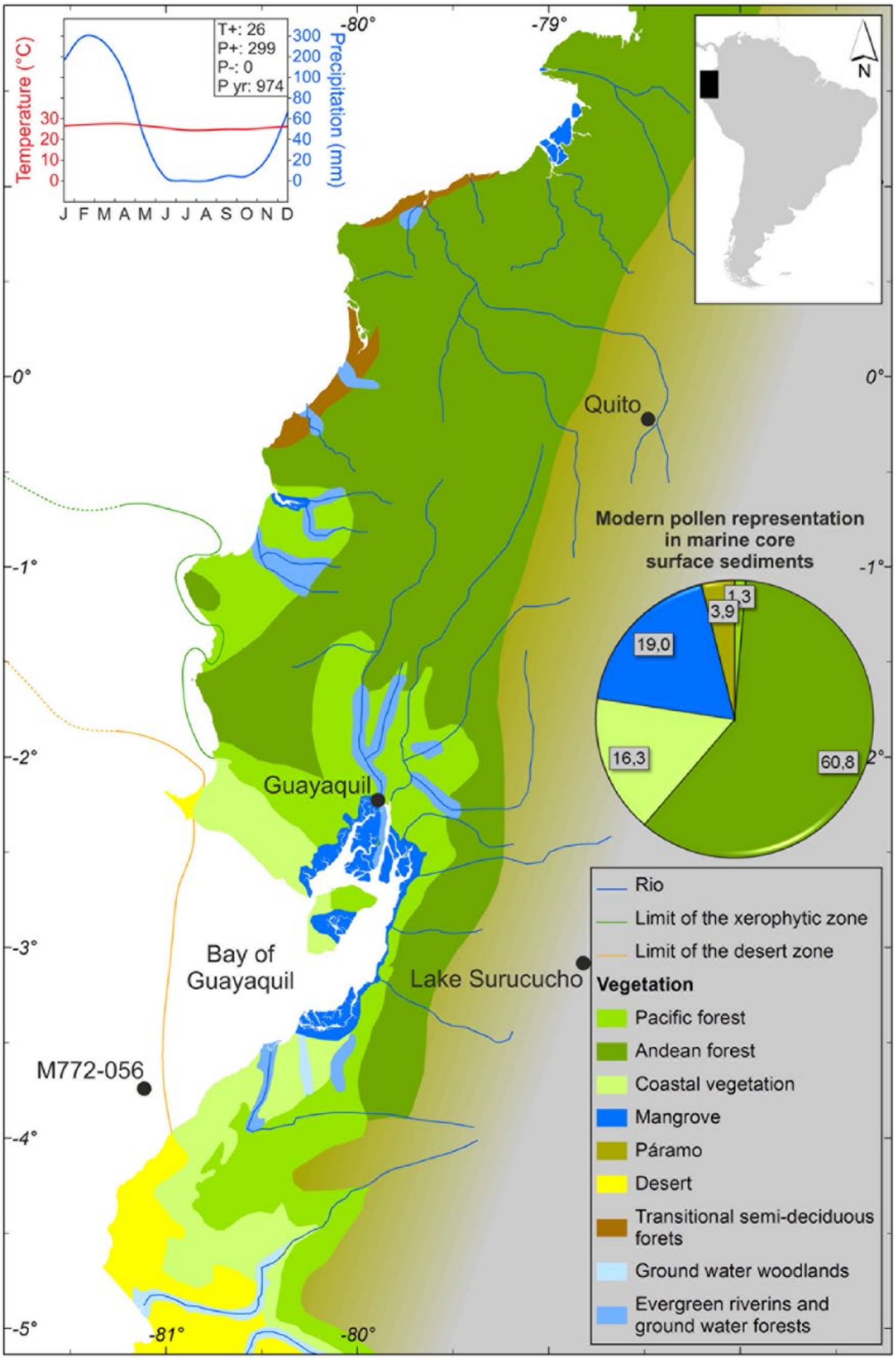


**Figure 1.** Map of the Guayaquil basin showing the distribution of the main vegetation types (redrawn from Troll, 1968). Top left: a pie diagram showing the pollen assemblage from the marine core M722-056 top sample that represents the different pollen percentages (numbers in black) of the vegetation communities (same colors as the map) occupying the Guayas basin during the last decades.

## Material and methods

### *The marine sedimentary sequence*

A piston core of 1062-cm length (M772-056, 03°44, 99′S, 81°07, 25′W, 350-m water depth) was drilled in 2008 in the southern part of the Bay of Guayaquil (Mollier-Vogel et al., 2013). This region is characterized by a sedimentary platform, the biggest sedimentary basin of the Andes, and the largest drainage system in western Ecuador (Stevenson, 1981), with an outer shelf break into the continental margin located at a water depth of ~100 m (Witt and Bourgois, 2010). This platform, which begins on the island of Puna and extends up to 100 km into the Ecuadorian inland and up to an elevation of more than 6000 m, resulted from a major subsidence phenomenon combined with an important sedimentary load of fluviomarine sediments from the estuary of the river Guayas. Today the sediments at the coring site are dominated by siliciclastic material, and secondarily they contain marine biogenic carbonates (Mollier-Vogel et al., 2013). Sedimentary discharge into the Gulf of Guayaquil is mainly linked to the Guayas River runoff, which integrates rainfall from a catchment located north of Guayaquil on the western flank of the Ecuadorian Andes (Twilley et al., 2001). The catchment area of this river drains the 32.674 km$^2$ (Figure 1) of the Guayaquil basin that represents 64% of the total drainage sediments (Rincón-Martínez et al., 2010).

**Table 1.** List of identified pollen taxa in marine core M772-056 (Guayaquil basin, Eastern equatorial Pacific) and clustering into groups after their main ecological affinity.

| Forest | | | Open vegetation | | |
|---|---|---|---|---|---|
| Mangrove | Pacific forest | Andean forest | Páramo | Coastal herbs and shrubs | Ubiquists |
| *Rhizophora* | Acanthaceae | *Alnus* | *Baccharis*-type (Asteraceae tubuliflorae) | *Acalypha* | Bromeliaceae |
| Acrostichum | *Alchornea* | Araliaceae | *Polylepis/Acaena*-type | *Ambrosia*-type | Cyperaceae |
| | Annonaceae | *Bocconia* | | Apiaceae *Daucus*–type | Fabaceae-type |
| | Araceae | Bromeliaceae | | Bromeliaceae | *Hedyosmum* |
| | Arecaceae-type | Caesalpiniaceae | | Campanulaceae | Melastomataceae |
| | Anacardiaceae | *Cerastium/Stellaria*-type | | *Cerastium/Stellaria*-type | Poaceae Scrophulariaceae |
| | *Banara*-type | *Clethra* | | Chenopodiaceae/Amaranthaceae-type | |
| | Bignoniaceae | *Clusiaceae* | | Cyperaceae | |
| | Bombacaceae | Convolvulaceae | | Ericaceae | |
| | Bromeliaceae | *Maripa*-type | | Gentianacea | |
| | Burseraceae-type | *Daphnopsis* | | Malvaceae | |
| | Cucurbitaceae | *Dodonaea* | | *Plantago* | |
| | *Dictyocaryum* | *Drimys* | | Poaceae | |
| | *Diospyros* | Ericaceae | | Polygonaceae | |
| | *Euphorbia/Mabea*-type | *Hedyosmum* | | Solanaceae | |
| | *Guazuma* | *Ilex* | | Ranunculaceae | |
| | *Hedyosmum* | *Juglans* | | *Taraxacum-type* (Asteraceae liguliflorae) | |
| | *Hyeronima* | Lamiaceae | | *Thalictrum* | |
| | *Iriartea* | Malpighiaceae | | | |
| | Loranthaceae | *Morella* (*Myrica*) | | | |
| | Meliaceae | Myrsine | | | |
| | *Mimosa* | Onagraceae | | | |
| | Myrtaceae | *Passiflora* | | | |
| | *Phyllanthus* | *Polylepis/Acaena*-type | | | |
| | Rubiaceae | *Podocarpus* | | | |
| | *Sapium* | Proteaceae | | | |
| | Sapotaceae | *Symplocos* | | | |
| | Sterculiaceae-type | *Vallea* | | | |
| | Ulmaceae | *Vicia* | | | |
| | Urticaceae/Moraceae-type | *Vismia* | | | |
| | | *Weinmannia* | | | |

The Guayas River discharge closely tracks the integrated precipitation and snow melting from the basin without any time lag (Twilley et al., 2001).

*Chronology.* The chronology of core M772-056 is based on 11 radiocarbon measurements on the planktonic foraminifera *Neogloboquadrina dutertrei* performed at the Leibniz Laboratory for Radiometric Dating and Stable Isotope Research, Kiel University (Mollier-Vogel et al., 2013; Table 2). $^{14}$C ages were converted into calendar ages using the CALIB 6.0 program (Stuiver and Reimer, 1993). Radiocarbon ages were first corrected using MARINE09 (Reimer et al., 2009), with a constant *R* of 200 ±50 years based on sites with known reservoir ages situated closest to our core location in the marine reservoir correction database (http://calib.qub.ac.uk/marine/). The age model was established by linear interpolation (Mollier-Vogel et al., 2013).

*Micropaleontological analyses.* A total of 125 silty-clay samples (between 4 and 10 cm$^3$) were taken at 10-cm intervals except for the upper 80 cm that covers the last millennium, where the sampling resolution was 5 cm. Pollen preparation follows the protocol detailed at (http://www.epoc.u-bordeaux.fr/index.php?lang=fr&page=eq_paleo_pollens). After chemical treatment (cold 10%, 25%, and 50% HCl, cold 45% and 70% HF, and then KOH), the samples were sieved through a 5-µm nylon mesh to concentrate the palynomorphs in the final residue. Two *Lycopodium* tablets with known concentration were added to each sample to calculate the pollen and spore concentrations. The final residue for pollen analysis was mounted unstained in bidistilled glycerine. Pollen grains were counted using a Zeiss Axioscope light microscope at 400× and 1000× (oil immersion) magnification. The identification of the different palynomorphs was based on a recent pollen reference collection held at the Institute of Evolutionary Science at the University of Montpellier, and on published morphological descriptions (Hooghiemstra, 1984; Roubik and Moreno, 1991). In most of the 125 samples analyzed, we counted more than 125 pollen grains, and between 25 and 40 morphotypes including herbs, shrubs, and trees. The pollen percentages for terrestrial taxa are based on a main pollen sum which excludes aquatics, unidentifiable (corroded, broken, crumpled), and unknowns. The percentages for fern spores, aquatics, unidentifiable, and unknowns are based on the total sum that corresponds to the main pollen sum *plus* fern spores, aquatics, unidentifiable, and unknowns. During this study, we identified and counted a total of 94 taxa, 18,207 pollen grains, and 3138 monolete and trilete pteridophyte spores. The 94 terrestrial spore and pollen taxa were grouped into six main groups according to their ecological affinities: the five vegetation types of the basin of Guayaquil: Páramo, coastal vegetation, mangrove, Andean and Pacific forests, and a group called ubiquitous that includes taxa that are found under several types of vegetation cover (Table 1). Pollen zones were originally established by visual inspection of the diagram and later confirmed by a constrained hierarchical clustering analysis based on Euclidean distance between samples. We used *chclst* function from the R package *Rioja* (Juggins, 2009).

## Results and interpretation

### *Long-term vegetation and climate changes in the Guayaquil basin during the Holocene*

The chronology of core M772-056 encompasses the very end of the late Glacial and the entire Holocene, from 12,300 cal. yr BP to the present. The sedimentation rate is relatively constant varying

**Table 2.** Radiocarbon dates ($^{14}$C-AMS) and sample specific data used for the age model of core M772-056 (Mollier-Vogel et al., 2013). Radiocarbon measurements were performed on the planktonic foraminifera *Neogloboquadrina dutertrei*.

| Labels | Depth (cm) | Sample material | Radiocarbon age ($^{14}$C yr BP) | Age range (cal. yr BP, 2σ) | Age mean value (cal. yr BP) |
|---|---|---|---|---|---|
| | 2 | | | | 0 |
| KIA 41276 | 49 | *N. dutertrei* | 1085 ± 25 | 416–616 | 516 |
| KIA 44035 | 138 | *N. dutertrei* | 2575 ± 30 | 1850–2153 | 2001 |
| KIA 41277 | 199 | *N. dutertrei* | 3255 ± 25 | 2717–2965 | 2841 |
| KIA 44036 | 338 | *N. dutertrei* | 4960 ± 30 | 4850–5225 | 5037 |
| KIA 41278 | 399 | *N. dutertrei* | 5510 ± 40 | 5563–5853 | 5708 |
| KIA 44037 | 508 | *N. dutertrei* | 6620 ± 35 | 6735–7088 | 6911 |
| KIA 41279 | 599 | *N. dutertrei* | 7430 ± 35 | 7574–7826 | 7700 |
| KIA 44038 | 693 | *N. dutertrei* | 8220 ± 60 | 8326–8678 | 8502 |
| KIA 41280 | 769 | *N. dutertrei* | 8960 ± 45 | 9271–9538 | 9404 |
| KIA 44039 | 893 | *N. dutertrei* | 10,085 ± 45 | 10,596–11,060 | 10,828 |
| KIA 41281 | 999 | *N. dutertrei* | 11,030 ± 50 | 12,052–12,561 | 12,306 |

between ~63 and 117 cm kyr$^{-1}$. The temporal resolution of the pollen analysis is one century on average ranging between 170 and 48 years. The last millennium has the finest resolution, that is, 60 years on average.

The interpretation of the pollen diagram was assisted by the analysis of the top core sample, taken at 3.5-cm core depth, that shows the pollen representation of the vegetation of the Guayaquil basin during the last decade (Figure 1). We observed that the pollen assemblage is mainly composed of arboreal pollen, including 60.8% of Andean forest (7.2% of *Alnus*) and 1.3% of Pacific rainforest, 19% of mangrove, 3.9% of Páramo, and 16.3% of coastal vegetation. These pollen percentages reflect the pollen production and proportion of the surface occupied by the five main vegetation communities of the Guayaquil basin and the efficiency of pollen transport to the ocean floor (Figure 1). Therefore, we consider that changes in the pollen record represent an integrated image of vegetation dynamics in the Guayaquil basin during the Holocene (Figure 2), and hence of the regional climate, as previously observed for other world regions (Dupont and Wyputta, 2003; Heusser, 1985; Hooghiemstra et al., 2006). The cluster analysis performed on the total counts show two major clusters that are in turn subdivided into two and three zones, respectively (Figure 2).

In the first cluster, 12,300–7700 cal. yr BP, we recognize two zones. The first zone, between 12,300 and 10,000 cal. yr BP, is characterized by the progressive increase and full development of the mangrove (*Rhizophora*) and Andean forest (*Alnus, Podocarpus, Morella (Myrica), Myrica, Myrsine*) while the coastal vegetation (Chenopodiaceae-type, *Acalypha*, and *Ambrosia*-type) progressively decreases. In the second zone, 10,000–7700 cal. yr BP, the mangrove started to decrease; the Andean forest shows a maximum while a reduction of the coastal vegetation is observed. Warmer and wetter conditions are revealed by this first cluster.

In the second cluster, from 7700 until the present, three zones can be recognized. The first zone from 7700 to 4200 cal. yr BP is characterized by a substantial increase of *Alnus* woodlands, the maximum proportion of *Podocarpus*, and a slow decrease in mangrove swamps reflecting relatively warm climate and the wettest conditions. The strong expansion of *Podocarpus, Alnus, Morella*, and fern spores in the Andean forest group is followed by their progressive decrease during this time interval while the coastal vegetation (Chenopodiaceae-type, *Acalypha*, and *Ambrosia*-type) expands. The mangrove forest shows low and high stands with a maximum development at 6000 cal. yr BP and two minima at 7500 and at 5600 cal. yr BP. Maximum warmth and humidity conditions reverse during this zone as reflected by the long-term substantial decrease of the Andean and mangrove forests. The second zone, between 4200 and 2850 cal. yr BP, is characterized by the maximum expansion of coastal vegetation, reduction of *Alnus* woodlands, the minimum percentages of the other Andean forest taxa (*Podocarpus, Morella, Myrsine*), and the lowest proportion of the mangrove taxa. This zone reveals the driest conditions in the Guayas basin. The third zone, from 2850 cal. yr BP to the present day, is a period characterized by a slight decrease but still high Páramo (*Baccharis*-type, *Acaena-Polylepis*-type) and coastal vegetation (Chenopodiaceae-type, *Acalypha*, and *Ambrosia*-type), and the increase of *Alnus* and mangrove. An alternation of increases and decreases in the Andean forest cover is inferred between 2850 and 850 cal. yr BP. This trend reverses with an increase of Andean forest from 850 cal. yr BP up to the present at the expense of both the Páramo and the coastal vegetation. A wet trend characterizes this time period.

Our marine pollen record M772-056 was compared with the closest terrestrial pollen record, that is, the Surucucho pollen sequence (Figure 3) located in the Guayaquil basin at more than 3000 m a.s.l. (Colinvaux et al., 1997; Weng et al., 2004). Both marine and terrestrial pollen sequences show similar fluctuations in the development of the *Alnus* forest. As already shown by the pollen analysis of the top-most core sample, the marine sequence records not only the coastal vegetation but also the vegetation occupying the river basin further inland and up to high altitudes. Andean alders reach their maximum expansion from 8000 cal. yr BP to the present, indicating warm and moist conditions at high altitudes, except between 4200 and 2850 cal. yr BP when *Alnus* woodlands declined synchronously with the Andean forest reduction (Colinvaux et al., 1997; Weng et al., 2004), reflecting the regional driest and coldest period of the Holocene.

### *Short-term vegetation and climate changes*

Superimposed to these long-term trends, our results suggest 29 short-term vegetation changes from Andean forest to coastal vegetation and back to forest (Figure 2).

The 3000-year period following the onset of the Holocene, 11,700–7700 cal. yr BP was interrupted by five multi-centennial cooling and drying events. These oscillations are inferred from the repeated contractions of the Andean forest: odd pollen subzones M772-1 and M772-3 and even pollen subzones M772-6 to 10. The first maximum of the Andean forest, M772-5, occurred at around 10,100 cal. yr BP, synchronous with the highest values of mangrove. Then, the mangrove contracted contemporaneously with a second maximum of Andean forest between 9700 and 9250 cal. yr BP (M772-7). Between 9250 and 9000 cal. yr BP, the Andean forest setback was associated with the maximum values of the Pacific forest (M772-8; Figure 2).

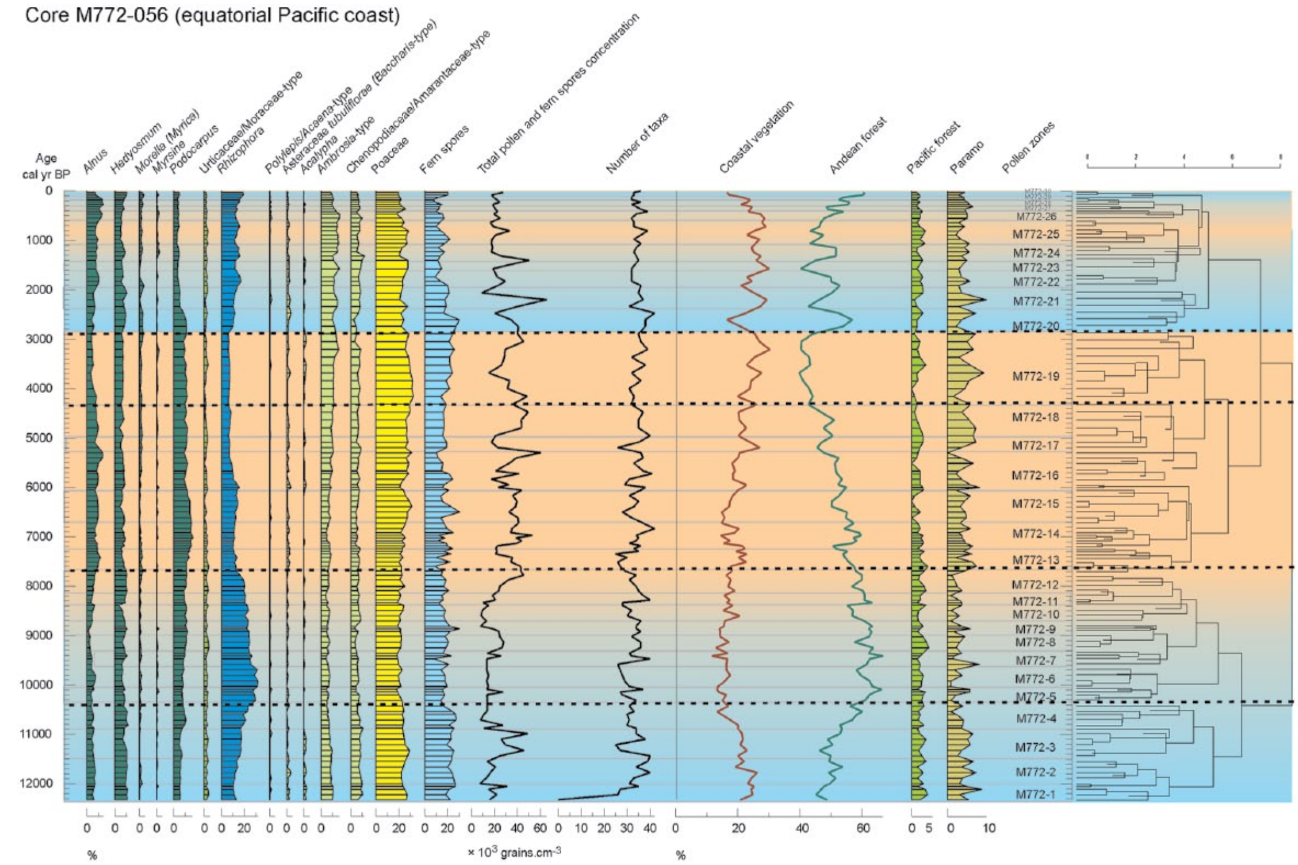


**Figure 2.** Pollen percentage diagram with selected taxa of core M772-056. Changes in pollen percentages are plotted against age. Dashed black lines indicate the five main pollen zones; gray solid lines indicate the pollen subzones. Blue and orange background for humid and dry conditions, respectively.

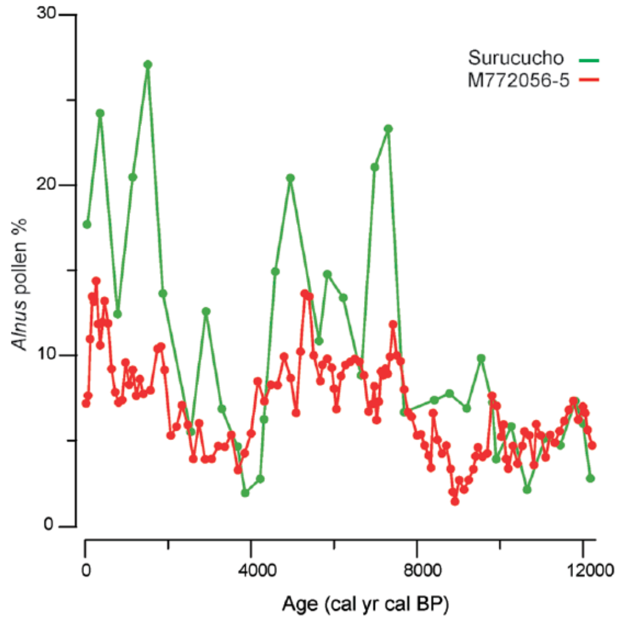


**Figure 3.** *Alnus* pollen percentage values along a time scale at Surucucho (Colinvaux et al., 1997) and in core M772-056.

The long-term regional drying trend from 7700 to 2850 cal. yr BP was punctuated by three multi-centennial dry events (Andean forest contractions at subzones M772, M772-14, and M772-15). After the driest period of the Holocene in Guayas, between 4200 and 2850 cal. yr BP, the third long-term phase marked by a wetter trend since 2850 cal. yr BP was interrupted by two dry intervals respectively at 2400–1950 and 1600–1400 cal. yr BP (subzones M772-21 and M772-23) marked by the reduction of both Andean forest and mangrove and a minima of *Podocarpus*. The last 1000 years have been analyzed at higher resolution (Figure 2) and despite coarser $^{14}C$ chronology for this interval, the M772-056 record suggests five regional vegetation changes that indicate an alternation of wetter and drier periods. The drier intervals 1000–750, 450–350, 200–100 cal. yr BP (M772-24, M772-26, and M772-28) are reflected by low or decreasing Andean forest, mangrove swamps, and *Alnus* woodlands. The most abundant presence of *Alnus* between 650 and 450 cal. yr BP and between 350 and 200 cal. yr BP (MM772-25 and 27) record moisture increase in the Guayas basin. In the last century, from 100 to 33 cal. yr BP (M772-29), we observe a simultaneous expansion of the mangrove and of the Andean forest, for the second time after the one observed at the beginning of the Holocene, which relates to a warming trend.

## Discussion

### *Related changes in vegetation and SST in the Guayaquil basin*

The interval between 12,000 and 10,000 cal. yr BP is characterized by the progressive development of the mangrove and the Andean forest with a maximum at around 10,000 cal. yr BP (Figure 4). Terrigenous input estimated from the same core (see log(Ti/Ca) in Figure 4) show high river discharges at the onset of the Holocene in agreement with the concomitant rapid and strong glacier melting observed in the Cordillera (Jomelli et al., 2011; Mollier-Vogel et al., 2013). The progressive decrease in terrigenous input after the early-Holocene peak of glacier melting suggests low precipitation on the continent. On the other hand, the increase of Andean forest suggests

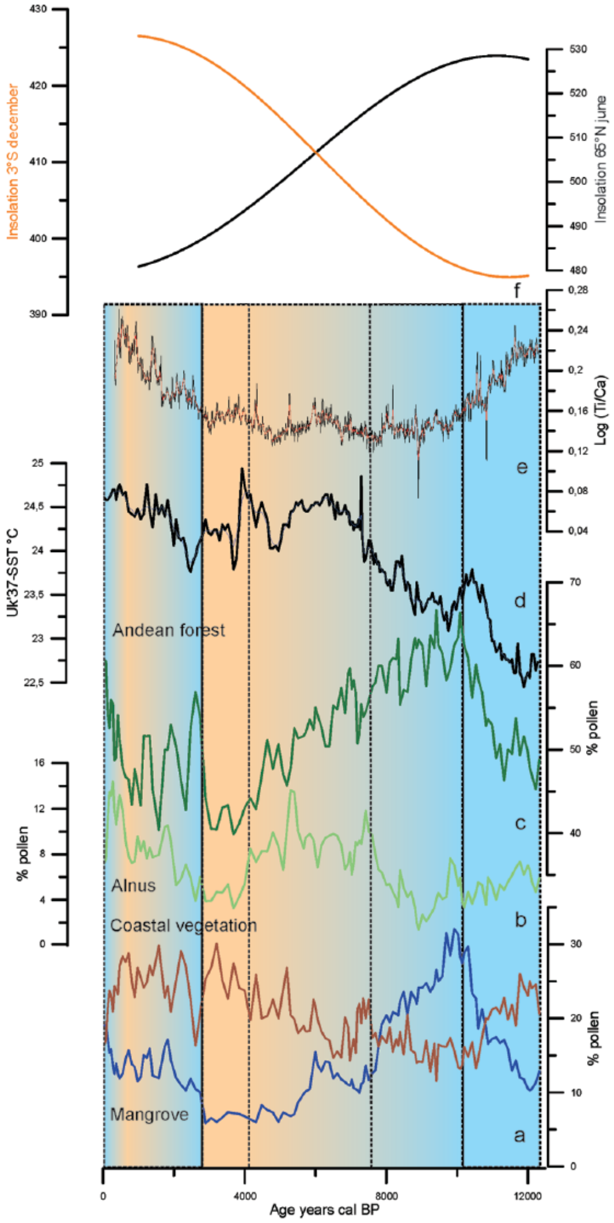


**Figure 4.** Direct comparison between SST changes in the Bay of Guayaquil and vegetation-based atmospheric changes in the Guayas basin from the analysis of core M772-056: (a) mangrove and coastal vegetation pollen percentage curves, (b) *Alnus* pollen percentage curve, (c) Andean forest pollen percentage curve, (d) $Uk'_{37}$-based SST changes (Mollier-Vogel et al., 2013), (e) Log(Ti/Ca) record, and (f) boreal (65°N) and austral (3°S) summer insolations (Berger, 1978). Blue and orange background for humid and dry conditions, respectively.
SST: sea surface temperature.

warming and higher moisture levels. However, the concomitant observed low *Alnus* percentages could characterize both cooling in coastal areas and a different moisture regime than that prevailing today with drier edaphic conditions and more cloud dripping. At the same time, SSTs remain low (Mollier-Vogel et al., 2013). Such divergences between coastal and highland temperatures are also observed in modern climate reconstructions with the development of a strong vertical stratification of temperature trends in the atmosphere (Vuille et al., 2015). This specific pattern of vegetation can be explained by the formation of fog and cloud condensation on the flanks of the Western Cordillera enhanced by a high temperature contrast between a cold sea and a warming land at the onset of the interglacial as already noticed by Jomelli et al. (2011).

Between 10,000 and 7700 cal. yr BP, Andean forest was continuously present although progressively decreasing. We know from the Atlantic side that the ITCZ was maintained in a northernmost position (Haug et al., 2001). In this study, relatively cold SSTs also show a weak influence of the ITCZ on the Pacific side at lower latitudes making a link with the ITCZ on the Atlantic. The position of the ITCZ to the north of our study area prevented the installation of a bimodal seasonality that would bring austral summer rainfalls. At Guayas during this time interval, the SST was warmer than during the previous time interval, the land–sea temperature contrast weaker, and the cloud formation on the continent less active. The climate became warmer and the continent progressively drier. The development of *Alnus* overall followed the progressive SST warming (Figure 4). This land–sea coupling can be related to the progressive increase of austral summer insolation at the latitude of Guayaquil.

Between 7700 and 4200 cal. yr BP, SSTs show maximum values. The vegetation was characterized by a maximum of *Alnus* and *Podocarpus* stands while the Andean forest cover continued to decrease. This opposite trend between *Alnus* and the rest of the Andean forest was also observed during the last glacial maximum (Mourguiart and Ledru, 2003). *Alnus* is a heliophilous species that requires less atmospheric moisture supply than the Andean forest although it benefits from azonal wet soils which may exist even under relatively low precipitation levels.

Mangrove swamps substantially decreased from 7700 cal. yr BP, and reached a minimum between ~5500 and ~2850 cal. yr BP that could indicate a decrease of SST due to the stronger penetration of the Humboldt Current in the bay or mean La-Niña-like conditions as observed in the southern Pacific (Carré et al., 2012). However, as the SST reached their highest values during this interval (Figure 4), the first hypothesis is rejected. Previous studies showed the tight link between fluctuations in the mangrove extent and sea level changes in the Caribbean region (Ellison and Stoddart, 1991; Parkinson et al., 1994). Therefore, mangrove contraction in the Bay of Guayaquil seems to respond preferentially to the reduction of marshlands because of a deceleration in sea level rise. Between 7700 and 6000 cal. yr BP, a slight re-expansion of the mangrove coincides with the stabilization of the sea level dated between 7000 and 6000 cal. yr BP (Lambeck and Chappell, 2001; Siddall et al., 2003), and the formation of a delta (Stanley and Warne, 1994). The maximum reduction of mangrove stands at ~5000 cal. yr BP was also documented in the Panamá basin, and interpreted as the replacement of the mangrove swamp by the lowland forest as the result of the sea level stabilization and the progradation of fluvial sediments (González et al., 2006). However, this second hypothesis does not explain the decrease in precipitation and the contraction of the Andean forest on the continent. Another hypothesis is that the southern shift of the ITCZ did not reach the latitude of Guayas during the austral summer and remained at a northern position as shown by the Cariaco record (Haug et al., 2001). The SSTs were warm, but the summer rainy season was weak or absent as shown by the low terrigenous input in the sediment. According to the study of Haug et al. (2001), the ITCZ started to move south after 5400 cal. yr BP which is also in agreement with the increase of river discharge into the Bay of Guayaquil (Figure 4). Therefore, we infer changes in sea levels that controlled the expansion of the mangrove on the coast and a weak influence of the ITCZ that prevented the expansion of the Andean forest on the flanks of the Western Cordillera during this interval.

From 4200 to 2850 cal. yr BP, the contraction of *Alnus*-dominated woodlands contemporaneously with the reduction of Andean forest and mangrove characterizes cooler and drier climatic conditions on the continent. Both the expansion of the coastal desert herbs, and particularly high-salinity tolerant plants such as Chenopodiaceae, and the cooler SSTs suggest a more northern influence of the Humboldt Current than today. The weak river discharges attest to low moisture rates on the continent. The influence of the ITCZ was still weak or absent and seasonal rainfall was reduced.

After 2850 cal. yr BP, the re-expansion of the Andean alders and of the mangrove swamp characterizes the return to warmer conditions on land. After a short cooling, SSTs also exhibit a warming trend. The Andean forest long-term decrease from ~2850 up to 1850 cal. yr BP can be explained by low-elevation cloud formation due to a weak land–sea temperature contrast. This trend reversed during the last two millennia which were marked by a rainfall increase. The last 2850 cal. yr BP was also punctuated by a high frequency and amplitude of contraction/expansion of different ecosystems, Andean forest, mangrove or coastal desert, with three alternated phases of major expansion – regression of the Andean forest versus coastal vegetation. The observed increase of *Alnus* woodlands over the last two millennia could also be explained by agroforestry as demonstrated in an Andean archeological site (Chepstow-Lusty and Winfield, 2000).

### *Orbitally driven climatic variability in the Guayaquil region*

The last 12,000 years are characterized by three steps in the amount of insolation (Figure 4). The first step shows maxima in the NH summer insolation and minima in SH summer insolation. The second step is a progressive increase of the insolation values in the SH with the associated progressive decrease in the NH. The third step is the reverse situation when comparing with the early Holocene.

In the early Holocene, the maximum summer insolation variations in the NH mid and high latitudes (Berger, 1978), and the progressive sea level rise associated with the last deglaciation, ended at ~7000 cal. yr BP. Between the early and late Holocene, the progressive decrease/increase of insolation values in the NH/SH is well reflected in the global trends of vegetation development with, for instance, the progressive decrease of Andean forests and mangroves and the increase of coastal vegetation. However, superimposed to this orbital forcing, variability in the SSTs and the mean position of the ITCZ bring some local effects in the climate and environmental features of the continent such as the dry phase observed between 4200 and 2850 cal. yr BP.

Our data indicate that long-term changes of the Andean forest cover were controlled by insolation variations at 65°N affecting the ITCZ position and related precipitation. The period between 4200 and 2850 cal. yr BP coincides with low boreal summer insolation but high summer insolation at 3°S, and shows a minimum development of Andean forest, mangrove, and *Alnus* synchronous with an optimal development of coastal vegetation and slightly lower SSTs. Insolation forcing drives the temperature gradients between low and high latitudes and consequently the position of the ITCZ. A southern migration of the ITCZ should induce a rainfall increase in the Guayaquil basin. However, we observe the driest conditions of the Holocene suggesting that the ITCZ was located further north, somewhere between 1°S and 3°S where high moisture rates are observed (Lim et al., 2014). This period, 4200–2850 cal. yr BP, also coincides with weaker ENSO frequency compared with the last 2000 years (Moy et al., 2002).

The third long-term phase, since 2850 cal. yr BP up to the present, is characterized by progressive, but irregular, increases in both SSTs and river discharge (terrigenous material) that followed the same trend as the SH summer insolation. Annual rainfall distribution responds to the southward ITCZ shifts that reached the latitude of Guayaquil and adopted the same bimodal seasonality as today (Figure 1). However, Andean forest, coastal vegetation, and mangrove do not follow the orbital trend and show high variability with an opposite pattern between, on the one hand, mangrove and Andean forest expansion and, coastal vegetation regression on the other hand.

### *Millennial-scale variability in the Guayaquil basin*

Superimposed to the orbitally driven climate variability, a succession of millennial-scale warm-wet/cool-dry intervals are recorded in the region of Guayaquil. Most of the regional forest cover contractions, indicating cooling/drying events, are contemporaneous with SST decreases that are weak, but larger than the error of the alkenone method (0.4°C; Pailler and Bard, 2002). We observe that the weak and low frequency ENSO events identified between 12,000 and 5000 cal. yr BP (Liu et al., 2014; Moy et al., 2002) coincide with muted Andean forest contraction/expansion in the Guayaquil basin (Figure 5). We also observe that the high variability and amplitude of the Andean forest changes are observed when ENSO frequency and amplitude increased, that is, during the last 3000 years (Figure 5). Based on Andean forest changes, a major increase of precipitation in the Bay of Guayaquil occurred at ~3000, 2000, and 1200 cal. yr BP which coincides with precipitation increase recorded at the Galapagos lake El Junco (Conroy et al., 2008). On the other hand, the coolest events observed at ~2500, 1500, and 1000 cal. yr BP in the Guayas basin are contemporaneous with cooling in the Bay of Guayaquil and could be related to a further northward penetration of the Humboldt Current along the coast of Peru. Therefore, we infer abrupt changes in the upwelling system driven either by the Humboldt Current or by ENSO at multi-decadal scales, or both, for the last millennia, thus reinforcing (or weakening) the average ITCZ-forced high (low) precipitations in the Guayas basin.

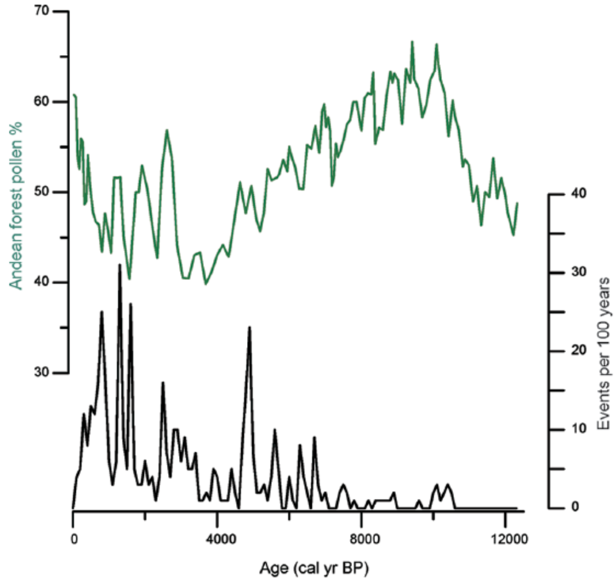


**Figure 5.** El Niño Southern Oscillation (ENSO) variability (Moy et al., 2002) and Andean forest pollen percentage curve (this study) during the Holocene.

### *The last 1000 years*

During the last 1000 years, the re-expansion of the glaciers during the ‘Little Ice Age’ (LIA) is associated with three dry phases interrupted by two wet phases (Ledru et al., 2013; Reuter et al., 2009). During this interval, we also observed in the Western Cordillera five changes in the development of Andean forest (Figure 6). Forest contraction, ~400–300 cal. yr BP, is inferred in the middle of the LIA bracketed by two periods of higher Andean forest cover indicating a one century dry event mimicking, within the chronological uncertainties, the climatic evolution already inferred from regional speleothem and other pollen records. These five intervals are also observed in the pollen record of Papallacta (00°21′30S; 78°11′37W) at an elevation of 3815 m a.s.l. They reflect changes in the Pacific Ocean SST and ITCZ shifts on both sides of the Andean Cordillera. Between 1000 and 750 cal. yr BP, the dry environment is related to low SST and low terrigenous deposits in the Bay of Guayaquil. At Cascayunga (Reuter et al., 2009), the moisture rates decrease showing that our records are in-phase and may display a

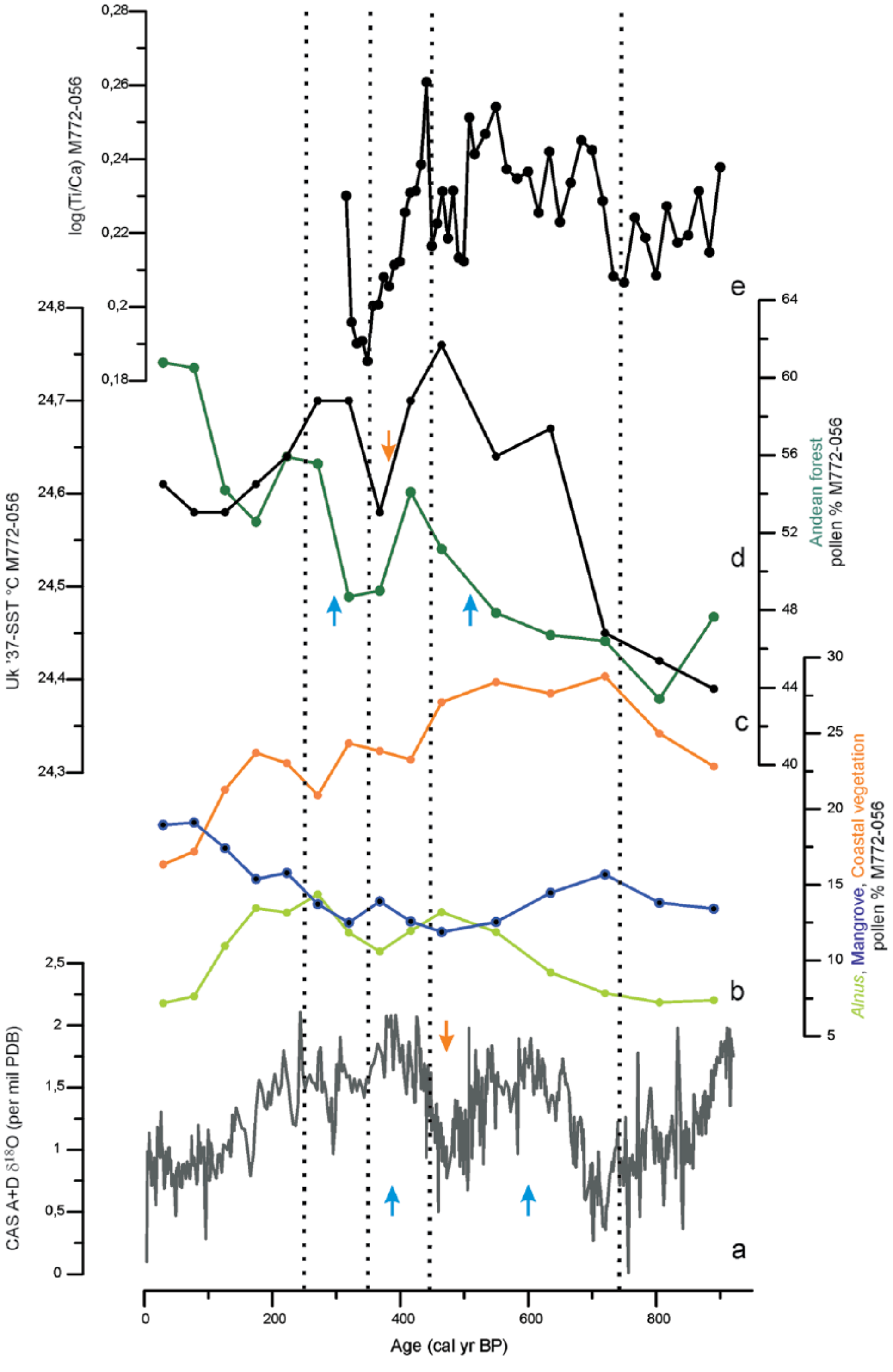


**Figure 6.** Precipitation changes during the last 1000 years on the eastern equatorial Pacific coastal region: (a) $\delta^{18}O$ speleothem record of Cascayunga (CAS A+D, Reuter et al., 2009), (b) *Alnus*, mangrove, and coastal vegetation pollen percentage curves from core M772-056, (c) Andean forest pollen percentage curve from core M772-056, (d) $Uk'_{37}$-based SST from core M772-056, and (e) log (Ti/Ca) curve from core M772-056. Blue and orange arrows show wet and dry phases during the 'Little Ice Age' (LIA), respectively. Black dashed lines indicate the three hydroclimate intervals based on terrigenous input in the Bay of Guayaquil discussed in the text.
SST: sea surface temperature.

regional climate trend. This interval reflects cold and dry climatic conditions during a high interdecadal ENSO variability and a northern position of the ITCZ that reduced the amount of rainfall at the latitude of Guayaquil.

Between 750 and 450 cal. yr BP, the high terrigenous are in phase with the high moisture rates as shown in the speleothem record in Cascayunga (Reuter et al., 2009). However, the Andean forest was not well developed during this interval and we rather infer a melting phase of the glacier at high elevation in phase with the high SST than higher precipitation rates on the Western Cordillera. Our pollen record also shows a development in the desert environment related to the strength of the Humboldt Current that could be related to the low interdecadal ENSO variability at low latitudes.

Between 450 and 350 cal. yr BP, the SSTs are decreasing and the terrigenous input is low reflecting cold and wet climatic conditions with a progressive drying trend along this interval. The ITCZ is reaching the latitude of Guayaquil at the beginning of the interval and progressively moving northward as attested by the following interval. Between 350 and 250 cal. yr BP, the vegetation, the low SST, and the low terrigenous input reflect the presence of stronger Humboldt Current and a weak influence of the ITCZ under low interdecadal ENSO variability. During this interval, the moisture rates were lower than in the previous phase on both sides of the Cordillera. This interval characterized the LIA in the Ecuadorian Andes (Ledru et al., 2013). After 250 cal. yr BP, the SST increase and the composition of the vegetation reflects the installation of a warm and wet climate on the continent. The moisture rates observed at Guayaquil are out of phase with the speleothem record of Cascayunga as were those of Papallacta on the Eastern Cordillera. A different origin for moisture, such as cloud dripping and upslope convective activity, was inferred at Papallacta to explain these differences between groundwater level (speleothem) and development of a wet forest on the slopes of the Cordillera (pollen records).

## Conclusion

Our marine record is well connected with the orbitally driven and SST-controlled climate changes of the tropical Andes (Jomelli et al., 2011; Polissar et al., 2013). Moreover, we assess the responses of the vegetation to these forcings and their associated ocean–atmosphere couplings on the equatorial Pacific coast and on the Western Cordillera. We confirm that marine pollen records collected from the river outlets represent an integrated image of the regional vegetation of the adjacent landmasses and, consequently, the climatic parameters under which this vegetation developed. We show that changes in insolation, SSTs, and ITCZ control the hydrological cycle in this area. Derived changes in the seasonality, in the strength of the Humboldt Current activity, and in multi-decadal scale ENSO variability show three main phases of ocean–atmosphere coupling during a continuous increase/decrease trend of austral/boreal summer insolation. These three climatic phases are associated with specific vegetation assemblages on the continent and more specifically on the Western Cordillera. During the early to middle Holocene, between 11,700 and 7700 cal. yr BP, climate conditions in the Guayas basin were controlled by the position of the ITCZ. The ITCZ was located further north and austral/boreal summer insolation was at a minimum/maximum. Precipitation was low but clouds formed on the Western Cordillera because of a warm land–cold sea thermal contrast while glaciers were rapidly melting in the Andes. This period coincides with simulated relatively weak ENSO strength. The progressive increase of SSTs, along the sea level rise, induced the full development of the mangrove in the Bay of Guayaquil. Between 7700 and 2850 cal. yr BP, the SSTs reached a maximum and showed high variability between two extreme cold events (at ~4500 and 3500 cal. yr BP) and one extreme warm event (~4000 cal. yr BP). The progressive southward shift of the mean position of the ITCZ had not yet reached the latitude of Guayaquil, and precipitation remained low on the Western Cordillera. The development of the vegetation is following the progressive increase/decrease of SH/NH summer insolation and is characterized by the regression of the Andean forest on the Western Cordillera while *Alnus* became more abundant. The simultaneous regression of the mangrove and expansion of the dry coastal vegetation suggest lower moisture rates, in agreement with model simulations (Braconnot et al., 2012), mainly related to the absence of the seasonal shift of the ITCZ at this latitude as the SSTs remained high and ENSO variability was low. The short interval between 4200 and 2850 cal. yr BP shows the coolest and driest climatic conditions of the Holocene. This interval reflects a northward shift of the Humboldt Current together with a northern position of the ITCZ. Between 2850 cal. yr BP and today, a high variability in the land–sea connections likely related with the high variability in frequency and strength of ENSO is documented by successive large expansion and contraction phases of the tropical forest and dry coastal vegetation. Pacific Ocean SSTs represent the main climate forcing with abrupt changes within the system such as those induced by ENSO. The continent became globally warmer and wetter with a strong variability during the latest part of the Holocene. The southern limit of the ITCZ reached the latitude of Guayaquil after 2500 years and induced the bimodal seasonal climate that still prevails today. We conclude that changes in equatorial Eastern Pacific Ocean SSTs and summer insolation are the main drivers of the composition of the ecosystems and the hydrological cycle of the Eastern Pacific coast and the Western Cordillera.

### Acknowledgements

We thank Henry Hooghiemstra and an anonymous referee for their insightful comments on the original manuscript. We are grateful to M. Georget for her technical assistance.

### Funding

Financial support for this study was provided by the French Research Agency ANR 2010 BLANC 608-01 ELPASO (MPL) project and the German Research Foundation through Collaborative Research Centre 754 'Climate-Biogeochemistry Interactions in the Tropical Ocean' (www.sfb754.de/en). The pollen data from this work can be found at http://doi.pangaea.de/10.1594/PANGAEA.849741.

### References

Barthlott W, Mutke J, Rafiqpoor MD et al. (2005) Global centres of vascular plant diversity. *Nova Acta Leopoldina* 92: 61–83.

Berger A (1978) Long-term variations of daily insolation and Quaternary climatic changes. *Journal of Atmospheric Science* 35: 2362–2367.

Braconnot P, Luan Y, Brewer S et al. (2012) Impact of Earth's orbit and freshwater fluxes on Holocene climate mean seasonal cycle and ENSO characteristics. *Climate Dynamics* 38: 1081–1092.

Cane MA (2005) The evolution of El Niño, past and future. *Earth and Planetary Science Letters* 230: 227–240.

Carré M, Azzoug M, Bentaleb I et al. (2012) Mid-Holocene mean climate in the south-eastern Pacific and its influence on South America. *Quaternary International* 253: 55–66.

Chepstow-Lusty A and Winfield M (2000) Inca agroforestry: Lessons from the past. *Ambio* 29: 322–328.

Clément AC, Seager R and Cane MA (2000) Suppression of El Niño during the mid-Holocene by changes in the Earth's orbit. *Paleoceanography* 15: 731–737.

Colinvaux PA, Bush MB, Steinitz-Kannac M et al. (1997) Glacial and postglacial pollen records from the Ecuadorian Andes and Amazon. *Quaternary Research* 48: 69–78.

Conroy JL, Overpeck JT, Cole JE et al. (2008) Holocene changes in eastern tropical Pacific climate inferred from a Galápagos lake sediment record. *Quaternary Science Reviews* 27: 1166–1180.

Dupont LM and Wyputta U (2003) Reconstructing pathways of aeolian pollen transport to the marine sediments along the coastline of SW Africa. *Quaternary Science Reviews* 22: 157–174.

Ellison JC and Stoddart DR (1991) Mangrove retreat with rising sea-level. *Journal of Coastal Research* 7: 151–165.

Garreaud RD, Vuille M, Compagnucci R et al. (2009) Present-day South American climate. *Palaeogeography, Palaeoclimatology, Palaeoecology* 281: 180–195.

González C, Urrego LE and Martínez JI (2006) Late Quaternary vegetation and climate change in the Panamá Basin: Palynological evidence from marine cores ODP 677B and TR 163–38. *Palaeogeography, Palaeoclimatology, Palaeoecology* 234: 62–80.

Haug GH, Hughen KA, Sigman DM et al. (2001) Southward migration of the intertropical convergence zone through the Holocene. *Science* 293: 1304–1308.

Heusser LE (1985) Quaternary palynology of marine sediments in the northeast Pacific, northwest Atlantic, and Gulf of Mexico. In: Bryant VM and Holloway RG (eds) *Pollen Records of Late-Quaternary North American Sediments*. Dallas, TX: American Association of Stratigraphic Palynologist, pp. 385–403.

Heusser LE and Balsam WL (1977) Pollen distribution in the N.E. Pacific Ocean. *Quaternary Research* 7: 45–62.

Hooghiemstra H (1984) Vegetational and climatic history of the high plain of Bogotá, Colombia. *Dissertationes Botanicae* 79: 1–368.

Hooghiemstra H, Lézine A-M, Leroy SAG et al. (2006) Late Quaternary palynology in marine sediments: A synthesis of the understanding of pollen distribution patterns in the NW African setting. *Quaternary International* 148: 29–44.

Jomelli V, Khodri M, Favier V et al. (2011) Irregular tropical glacier retreat over the Holocene epoch driven by progressive warming. *Nature* 474: 196–199.

Jorgensen PM and Leon-Yanez S (1999) *Catalogue of the Vascular Plants of Ecuador*. St. Louis, MO: Missouri Botanical Garden.

Juggins S (2009) *Package 'rioja' – Analysis of Quaternary Science Data*. The Comprehensive R Archive Network.

Lambeck K and Chappell J (2001) Sea level change through the last Glacial Cycle. *Science* 292: 679–685.

Ledru M-P, Jomelli V, Samaniego P et al. (2013) The Medieval Climate Anomaly and the Little Ice Age in the Eastern Ecuadorian Andes. *Climate of the Past* 9: 307–321.

Leduc G, Vidal L, Tachikawa K et al. (2009) ITCZ rather than ENSO signature for abrupt climate changes across the tropical Pacific? *Quaternary Research* 72: 123–131.

Lim S, Ledru M-P, Bremond L et al. (2014) Ecological effects of natural hazards and human activities on the Ecuadorian Pacific coast during the late Holocene. *Palaeogeography, Palaeoclimatology, Palaeoecology* 415: 197–209.

Liu Z, Lu Z, Wen X et al. (2014) Evolution and forcing mechanisms of El Niño over the past 21,000 years. *Nature* 515: 550–553.

Marchant R, Almeida L, Behling H et al. (2002) Distribution and ecology of parent taxa of pollen lodged within the Latin American Pollen Database. *Review Paleobotany and Palynology* 121: 1–75.

Mollier-Vogel E, Leduc G, Böschen T et al. (2013) Rainfall response to orbital and millennial forcing in northern Perú over the last 18 ka. *Quaternary Science Reviews* 8: 125–141.

Morales MS, Christie DA, Villalba R et al. (2012) Precipitation changes in the South American Altiplano since 1300 AD reconstructed by tree-rings. *Climate of the Past* 2: 653–666.

Mourguiart P and Ledru M-P (2003) Last glacial maximum in an Andean cloud forest environment (Eastern Cordillera, Bolivia). *Geology* 31: 195–198.

Moy CM, Seltzer GO, Rodbell GT et al. (2002) Variability of El Niño/Southern Oscillation activity at millennial timescales during the Holocene epoch. *Nature* 420: 162–165.

Pailler D and Bard E (2002) High frequency palaeoceanographic changes during the past 140,000 yr recorded by the organic matter in sediments of the Iberian margin. *Palaeogeography, Palaeoclimatology, Palaeoecology* 181: 431–452.

Parkinson RW, Delaune RD and White RJ (1994) Holocene sea-level and the fate of mangrove forests within the wider Caribbean region. *Journal of Coastal Research* 10: 1077–1086.

Polissar PJ, Abbot MB, Wolfe AP et al. (2013) Synchronous interhemispheric Holocene climate trends in the tropical Andes. *Proceedings of the National Academies of the United States of America* 110(36): 14551–14556.

Reimer PJ, Baillie MGL, Bard E et al. (2009) IntCal09 and Marine09 radiocarbon age calibration curves, 50,000 years cal BP. *Radiocarbon* 51: 1111–1150.

Reuter J, Stott L, Khider D et al. (2009) A new perspective on the hydroclimate variability in northern South America during the Little Ice Age. *Geophysical Research Letters* 36: L21706.

Riedinger MA, Steinitz-Kannan M, Last WM et al. (2002) A ~6100 $^{14}C$ year record of El Niño activity from the Galápagos Islands. *Journal of Paleolimnology* 27: 1–7.

Rincón-Martínez D, Lamy F, Contreras S et al. (2010) More humid interglacials in Ecuador during the past 500 kyr linked to latitudinal shifts of the equatorial front and the Intertropical Convergence Zone in the eastern tropical Pacific. *Paleoceanography* 25: PA2210.

Rodbell D, Seltzer GO, Anderson DM et al. (1999) A 15,000 year record of El Niño driven alluviation in southwestern Ecuador. *Science* 283: 516–520.

Roubik DW and Moreno E (1991) *Pollen and Spores of Barro Colorado Island* (Monographs in Systematic Botany, vol. 36). St. Louis, MO: Missouri Botanical Garden.

Schneider T, Bischoff T and Haug G (2014) Migrations and dynamics of the intertropical convergence zone. *Nature* 513: 45–53.

Siddall M, Rohling EJ, Almogi-Labin A et al. (2003) Sea-level fluctuations during the last glacial cycle. *Nature* 423: 853–858.

Stanley DJ and Warne AG (1994) Worldwide initiation of Holocene marine deltas by deceleration of sea-level rise. *Science* 265(5169): 228–231.

Stevenson MR (1981) *Seasonal Variations in the Gulf of Guayaquil, A Tropical Estuary* (Boletin Científico y Técnico, vol. 4). Guayaquil: Instituto Nacional de Pesca, 133 pp.

Stuiver M and Reimer PJ (1993) Extended 14C database and revised CALIB radiocarbon calibration program. *Radiocarbon* 35: 215–230.

Troll C (1968) *Geoecologia de las regions montañosas de las Américas tropicales* (Colloquium Geographicum, vol. 9). Bonn: Dummlers Verlag, 223pp.

Tudhope AW, Chilcott CP, McCulloch MT et al. (2001) Variability in the El Nino-Southern Oscillation through a glacial-Interglacial Cycle. *Science* 291: 1511–1517.

Twilley RR, Cárdenas W, Rivera-Monroy VH et al. (2001) The Gulf of Guayaquil and the Guayas River estuary, Ecuador. In: Seelinger U and Kjerfve B (eds) *Coastal Marine Ecosystems in Latin America* (Ecological Studies, vol. 144). Berlin: Springer, pp. 245–264.

Urrego DH, Silman MR, Correa-Metrio A et al. *(2011)* Pollen-vegetation relationships along steep climatic gradients in western Amazonia. *Journal of Vegetation Science* 22: 795–806. 10.1111/j.16541103.2011.01289.x.

Vuille M, Bradley RS and Keimig F (2000) Climate variability in the Andes of Ecuador and its relation to tropical Pacific and Atlantic Sea surface temperature anomalies. *Journal of Climate* 13: 2520–2535.

Vuille M, Franquist E, Garreaud R et al. (2015) Impact of the global warming hiatus on Andean temperature. *Journal of Geophysical Research* 120: 3745–3757.

Weng C, Bush MB and Cheptow-Lusty AJ (2004) Holocene changes of Andean alder (Alnus acuminata) in highland Ecuador and Peru. *Journal of Quaternary Science* 19: 685–691.

Witt CS and Bourgois J (2010) Forearc basin formation in the tectonic wake of a collision-driven, coastwise migrating crustal block: The example of the North Andean block and the extensional Gulf of Guayaquil-Tumbes Basin (Ecuador-Peru border area). *Geological Society of America Bulletin* 122: 89–108.

Wyrtki K (1975) EL Niño – The dynamic response of the equatorial Pacific Ocean to atmospheric forcing. *Journal of Physical and Oceanography* 5: 572–584.